Commun Nonlinear Sci Numer Simulat 64 (2018) 122–134

Contents lists available at ScienceDirect

Commun Nonlinear Sci Numer Simulat

journal homepage: www.elsevier.com/locate/cnsns

Research paper

Experimental evidence of power law reinjection in chaotic intermittency

Ezequiel del Rio[a,*], Sergio Elaskar[a,b]

[a] Dpto. Física Aplicada. ETSI Aeronáutica y del Espacio. Universidad Politécnica de Madrid, Plaza Cardenal Cisneros 3. 28040 Madrid, Spain

[b] Departamento de Aeronáutica, FCEFyN Universidad Nacional de Córdoba, Instituto de Estudios Avanzados en Ingeniería y Tecnología CONICET and Universidad Nacional de Córdoba, Argentina

ARTICLE INFO

Article history:
Received 15 December 2017
Revised 22 March 2018
Accepted 11 April 2018
Available online 16 April 2018

Keywords:
Chaos
Intermittency
Noise
Analog circuit

ABSTRACT

The main classical results on classical chaotic intermittency were based on a uniform reinjection on the laminar region. Recently, for a wide class of 1D maps, a generalized power law reinjection was found, so the classical theory of intermittency was generalized for 1D-maps. We propose experimental evidences that this generalization works also in an experiment based on an analog circuit. In the noisy case, we also found good agreement with a recently proposed theory for this scenario.

1. Introduction

Intermittency is a particular route to the deterministic chaos characterized by spontaneous transitions between laminar and chaotic dynamics. For the first time this concept has been introduced by Pomeau and Maneville in the context of the Lorenz system [1,2]. Later intermittency has been found in a variety of different systems including, for example, periodically forced nonlinear oscillators, Rayleigh-Bénard convection, derivative nonlinear Schrödinger equation, and in development of turbulence in hydrodynamics (see e.g. Refs. [3,4]). Proper qualitative and quantitative characterizations of intermittency based on experimental data are especially useful for studying problems with partial or complete lack of knowledge on exact governing equations, as it frequently happens e.g. in Economics, Biology, and Medicine (see e.g. Refs. [5,6]). In this case special attention has to be payed to the length of data sets required for robust estimation of the model parameters.

According to Pomeau and Manneville, intermittency can be classified into three types depending on the local geometry of their Poincaré map: type-I for quadratic maps and type-II and type-III for cubic ones [7]. However, other non linear types had been reported [8–10], hence the local laminar dynamics of type-I intermittency is determined by the 1D map in the form :

$$x_{n+1} = \varepsilon + x_n + a\, x_n^p \qquad \text{Type-I} \tag{1}$$

* Corresponding author.
E-mail address: ezequiel.delrio@upm.es (E.d. Rio).

https://doi.org/10.1016/j.cnsns.2018.04.013
1007-5704/

where $a > 0$ accounts for the weight of the nonlinear component determined by the exponent p. The laminar behavior of type-II and type-III are described by the maps:

$$x_{n+1} = (1+\varepsilon)x_n + ax_n^p \qquad \text{Type-II} \tag{2}$$

$$x_{n+1} = -(1+\varepsilon)x_n - ax_n^p \qquad \text{Type-III} \tag{3}$$

In all the types, the fixed point of the system becomes unstable for positive values of the parameter ε. Traditionally was used $p = 2$ for type I intermittency and $p = 3$ for type II and III. However, those restrictions are actually not necessary [11]. Another condition for a one-dimensional map to possess intermittency is to have a reinjection mechanism mapping back the trajectories from the chaotic zone into the laminar one. This mechanism is described by the so-called reinjection probability density (RPD), which is determined by the chaotic dynamics of the system itself. The function RPD together with the local map determine all the dynamical properties of the system. In general it is difficult to get an analytical expression for the RPD, hence different approximation have been used. The most common approximation used to obtain many classical results on intermittency theory have been to consider the RPD uniform. and thus independent of the reinjection point [3,7,12–17], however, works fine in a few model cases only [12,14,16]. Another approach deals with the other limit, δ-function like RPD. It considers reinjection into a given point in the presence of noise [15,18].

Recently to describe the reinjection mechanism of a wide class 1D maps exhibiting intermittency it was introduced a generalized RPD, a parametric power law function depending on a free parameter $m \in (0, 1)$. The generalized RPD includes the uniform reinjection as a particular case $m = 1/2$ [9,19]. We showed that the shape of the generalized RPD is determined by the behavior of trajectories within chaotic regime in a vicinity of a point in the Poincare map with infinite or zero tangent [20].

The shape of the new RPD enables analytic estimation the fundamental characteristic of the intermittency, that is, the probability density of the length of laminar phase $\psi(l)$ where l approximates the number of iterations in the laminar region, i.e. the length of the laminar phase. Note that, as the function $\psi(l)$ can be estimated for time series, it is usually used to identify the intermittency type by comparing with the analytic estimation.

The new RPD has been found in many 1D map and the analytical predictions for RPD and for$\psi(l)$ have been numerically confirmed even in the pathological cases of intermittency described in the literature. This case are known by their signiant deviation of the main characteristics (e.g. the length of the laminar phase) from those predicted by the classical theory. It have been shown that the generalized reinjection probability density provides faithful description of anomalous and standard intermittencies in the unified framework [20,22].

Because the noise is always present in experiments, it is of a fundamental importance to know the effect of noise on the intermittency phenomenon, in particular on the RPD. There are many papers devoted to study noise effect on chaotic intermittency, by means of the normalization group analysis [8], or by using the Fokker–Plank equation [17,18,26,27] among the others. Note that, in spite of the fact that the noise affects the whole region where the system dynamics takes place, classically, the researches are devoted to the noise effect on the laminar region of the Poincaré map and there was no study in classical theory of intermittency focused on the effect of noise on the RPD.

Actually, the RPD described by a power law introduces a novel scenario because, whereas the classical uniform reinjection should remain constant under a wide class of noise distributions, the new RPD can be affected by the noise. For 1D-map, recently an analytical approach to the noise reinjection probability density (NRPD) has been present [23–25,28]. Note that the probability density of the laminar lengths $\psi(l)$ depend on the reinjection probability density, hence the NRPD also determines a noisy $\psi(l)$. For a review of the generalized theory see [11].

The theory of intermittency sketched before has been developed for 1D map. However, continuous systems that contract volume in phase spaces can be described by the 1D maps [29], hence, it is possible, at least theoretically, to extend the new intermittency framework to continuous systems. In spite of that, there is has not been reported experimental confirmation in continuous systems.

This demands further investigations. In this paper we apply the previously described the intermittency theory to experimental data coming from an analog circuit. We provide an experimental confirmation of the relevant results of the new intermittency theory. In particular, The RPD base on a power law found in a wide class of 1D map also describe accurately the reinjection found experimentally in our continuous system. Moreover, the aims of this paper is also to show that the RPD observed in experimental continuous dynamical systems is affected by the noise of the system as it has recently been analytically and numerically reported for 1D-maps.

The rest of the paper is organized as follows. The Section 2 is devoted to make a brief introduction of the intermittency theory that we need to evaluate the experimental result. In Section 3 we present the model and the experimental setup. Section 4 deals with the experimental Poincaré map. Results on the experimental noiseless power law RPD are present in Section 5 whereas Section 6 is devoted to the noisy case. The mains conclusions are present in Section 7.

2. Mathematical background

Before embarking in the experiment description, let us summarize the concept that we will used to analyze the experimental results. In absence of noise, the generalized RPD is given by the next power law [9,10,19].

$$\phi(x) = b(x - \hat{x})^{\alpha} \tag{4}$$

witch drives the reinjection mechanism for a number of maps having intermittencies of the type I, II and III. The RPD (4) has two free parameters $\hat{x}$ and α determined by the dynamics in the chaotic region. The parameter $\hat{x}$ corresponds with the so-called lower bound of reinjection (LBR), that is $\hat{x} \leq x$, and it can strongly determines the dynamical behavior of the map (see for instance [19,21–24]). The symmetry case where, that is $x \leq \hat{x}$, can be take into account by substituting in the RPD (4) $(x - \hat{x})$ by $(\hat{x} - x)$. As the following results can be extended in a natural way to the symmetry case, for sake of clarity, in this work we consider only the RPD given by Eq. (4).

The exponent α is determined by the geometry of the map in a vicinity of a point with infinite or zero tangent, and b is determined by the normalization condition.

$$\int_{\hat{x}}^{c} b(x - \hat{x})^{\alpha} dx = 1. \tag{5}$$

Where c determines the upper limit of the laminar zone. Note that the RPD (4) includes the constant reinjection approach as the particular case $\alpha = 0$. Recently has been proposed an analytical procedure to obtain the value of α from the analytical expression of the map [20]. For some celebrated classical maps having intermittency, this method predicts the complete statistical behavior already found by numerical investigation.

On the other hand, a simple methodology to evaluate the free parameters $\hat{x}$ and α from numerical or experimental data has been proposed by using the function $M(x)$ defined as

$$M(x) = \begin{cases} \frac{\int_{x_s}^{x} \tau\, \phi(\tau)\, d\tau}{\int_{x_s}^{x} \phi(\tau)\, d\tau} & \text{if } \int_{x_s}^{x} \phi(\tau) d\tau \neq 0 \\ 0 & \text{if } \int_{x_s}^{x} \phi(\tau) d\tau = 0, \end{cases} \tag{6}$$

where x_s is a suitable starting point having $x_s < x$ for all reinjected point x. The domain of definition of $M(x)$ is the laminar region. As $M(x)$ is defined by means of integrals, it is easier to compute than $\phi(x)$, and also the effects coming from the statistical fluctuations are reduced, even for a relatively low number of data [22]. Moreover, note that for a given value of x, $M(x)$ is the average of reinjection points in the interval (x_s, x), hence, if we sort the reinjections according to the relation $x_j < x_{j+1}$, a simple estimation of the function $M(x)$ is obtained by means of

$$M(x_l) \approx \frac{\sum_{j=1}^{l} x_j}{l}, \tag{7}$$

which has been used in this work to evaluate the function $M(x)$ instead of using the definition Eq. (6).

An important property of the function $M(x)$ is that for the RPD given by Eq. (4), it becomes linear as follow

$$M(x) = \begin{cases} m(x - \hat{x}) + \hat{x} & x > \hat{x} \\ 0 & otherwise \end{cases} \tag{8}$$

where the exponent α is determined by the slope m, hence the RPD is given by

$$\phi(x) = b(x - \hat{x})^{\alpha} \quad \text{where} \quad \alpha = -\frac{1 - 2m}{1 - m}, \tag{9}$$

Assuming $\alpha > -1$, that is $0 < m < 1$, Eq. (5) converges.

According to Eq. (9), the particular value $m = 1/2$ correspond to the classical approach $\phi(x) = cte$ considered in the literature. On the other hand, the RPD (9) has two limit cases:

$$\phi_0(x) = \lim_{m \to 0} \phi(x) = \delta(x - \hat{x}) \tag{10}$$

$$\phi_1(x) = \lim_{m \to 1} \phi(x) = \delta(x - c) \tag{11}$$

In the limit (10) the reinjection is mainly concentrated on the single point $\hat{x}$, whereas in the second limit the reinjection is concentrated on an endpoint of the laminar region.

least mean square fit

Note that by a simple least mean square fit, Eq. (8) provides the parameters $\hat{x}$ and α determining the RPD. Let us describe how the RPD affects the duration of the laminar phase. An important quantity related to the intermittency phenomenon is the probability density of the laminar lengths $\psi(l)$, being $\psi(l)\, dl$ the probability of finding a laminar phase of a given length lying between l and $l + dl$, where l indicates the number of iterations in the laminar region.

To determine $\psi(l)$ we follow the classical approach [7], and we approximate the dynamics of the local map by a differential equation. The appropriated equation to model the local behavior of the experiment described below is Eq. (3) with $p = 2$, so the approximate differential equation is given by

$$\frac{d|x|}{dl} = \varepsilon |x| + a|x|^2. \tag{12}$$

By solving the above equation we obtain

$$l(|x|, c) = \int_{|x|}^{c} \frac{dz}{\varepsilon\, z + a\, z^2} = \frac{1}{\varepsilon}\left[\ln\left(\frac{c}{|x|}\right) - \ln\left(\frac{\varepsilon + a\, c}{\varepsilon + a\, x}\right)\right], \tag{13}$$

which is referred to a local behavior of the map in the neighborhood around of the unstable fixed point.

Now, the probability density of the laminar lengths $\psi(l)$, is given by

$$\psi(l) = \phi(X(l,c))\left|\frac{dX(l,c)}{dl}\right|, \tag{14}$$

where $X(l, c)$ is $l^{-1}(x, c)$, the inverse function of $l(x, c)$ in Eq. (13) with respect to its first argument, that is,

$$X(l,c) = \frac{\varepsilon}{(a+\varepsilon/c)e^{\varepsilon l} - a}. \tag{15}$$

Taking into account the Eq. (12) and the above relations, we finally have

$$\psi(l) = \phi(X(l,c))\left[aX(l,c)^2 + \varepsilon X(l,c)\right]. \tag{16}$$

An important difference with the classical approach is the factor $\phi(X(l, c))$ in Eq. (16), hence, the $\psi(l)$ depends not only on the local laminar map described by $X(l, c)$ but also on the chaotic one, described by the factor $\phi(X(l, c))$.

We would like to point out that to derive Eq. (16) was necessary used a continuous approximation for obtain Eq. (12). This procedure works perfectly for very low values of ε, but in other cases such approximation can introduce some error.

2.1. The noise effect

In summary, the noisy NRPD (denoted here by capital case $\Phi(x)$, whereas the lower case $\phi(x)$ denotes the noiseless RPD) is given by

$$\Phi(x) = \int \phi(y)G(x-y,\sigma)\mathrm{d}y \tag{17}$$

where $G(x-y,\sigma)$ in the probability density of the internal noise depending on the noise strength parameter σ.

In our experimental setup, $G(x-y,\sigma)$ and σ should be referred to the experimental Poincaré map and they are, in general, unknown.

It is important to note that Eq. (17) describes how the noise in the experimental Poincaré map transforms the noiseless RPD, $\phi(x)$ to the noisy RPD $\Phi(x)$.

Note that in the noiseless case, $\phi(x)$ is determined by $M(x)$ and it is given by Eq. (9). However, spite of the experiment is carried out in noisy condition, the function $M(x)$, which is evaluated considering data not too close to the fixed point, still provides the parameters α and $\hat{x}$ that determine $\phi(x)$ in Eq. (17) [28]. In Section 6 we obtain $\phi(x)$ from the nosily data and we propose an explicit function for $\Phi(x)$. After $\Phi(x)$ is evaluated, to estimate the noisy probability density of the laminar length we can use the Eq. (16) where the substitution $\phi(x)$ by $\Phi(x)$ is required.

3. The model and the circuit

3.1. The model

In the following sections we apply the analytical result previous described to an experimental analog circuit. We are interested in the experimental Poincaré map and in the RPD observed in such map with and without noise. We will compare with the analytical prediction previously described.

First of all, let us briefly review some relevant experiments carry out on chaotic intermittency. Note that classically, the RPD generated in the chaotic region of the Poincaré map was consider uniform, hence the important region was the laminar one. This is because, in many experimental papers on intermittency, the experimental Poincaré map is not reported (see for instance [30–33]) or it is reported only the local experimental Poincaré map as it has happened for instance in [3,6,34]. Note that in these cases, it can be observed a gate around the unstable point of the local map. This is a global effect on the reinjection into the laminar region that suggest that the RPD is not uniform.

In the case where the total experimental Poincaré map is reported, it looks very complex, [15,16,35–37], hence the reinjected points come from many different region (multi-reinjection) as can be observed in [21] for the fifth interaction of the Poincaré map. The opposite case can be represented by the very simple map shown in [38]. However, in this case the reinjection is coming from a region without extreme points, hence an uniform reinjection is expected, that corresponds with the classical scenario. According with the introduction section, our interest is to find an experiment showing a simple Poincaré map presenting a reinjection mechanism driven by the neighborhood of an extreme point.

A continuous model with the mentioned requirements is described by the follow third order differential equation.

$$\frac{\mathrm{d}^3 z}{\mathrm{d}\tau^3} + d_2\frac{\mathrm{d}^2 z}{\mathrm{d}\tau^2} + d_1\frac{\mathrm{d}z}{\mathrm{d}\tau} + d_0 z - D_z(z) + 1 = 0 \tag{18}$$

where d_i $(i = 0, 1, 2, 3)$ are constant coefficients and $z(\tau)$ and τ account for a dimensionless variable and dimensionless time, whereas $D_z(z)$ is defined by the piecewise linear function given by

$$D(z) = \begin{cases} -kz & if \quad z \le 0 \\ 0 & otherwise \end{cases} \tag{19}$$

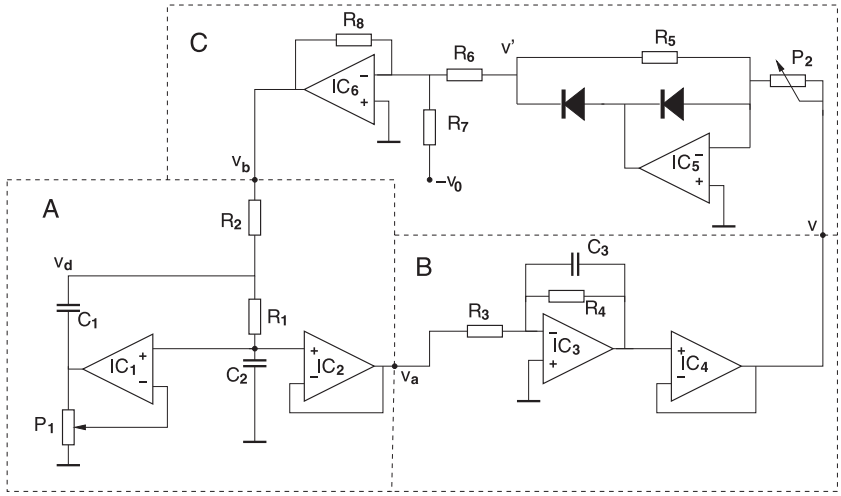

Fig. 1. Circuit used to model the Eq. (25). Dashes lines divide the circuit in three parts labeled *A*, *B* and *C*. The nominal value of all the resistors is $R = 10$ kΩ except for R_4 that is 10 MΩ and $P_1 = 5$ kΩ. The nominal value of the capacitors is $C_1 = C_2 = C_3 = C = 0.1$ μF. We use OP27 operational amplifier chosen for their low noise and the diode type is 1n4148. IC_2 and IC_4 work as voltage followers.

where k is a constant. As will see below, the value of d_0 is much lower than the rest of the parameter values, hence in good approximation the system (18) is the same which is considered in [39]. Also the proposed circuit to mimic Eq. (18) is based in Ref. [39].

We have chosen the model (18) because it presents a simple Poincaré map with reinjection determined from a local maximum of the map as we can see below. Our theory can be applied to more complex maps, but for sake of clarity we prefer the most simple one to study the theory in an experimental continuous system.

Other important advantages of the model is its no-linear part. It is electronically simple to mimic it and it permits to scale the Eq. (18). This fact will be very important to study the noise effect in a natural way, that is, by using the internal noise of the circuit.

3.2. The circuit

The Eq. (18) is modeled by the circuit shown in Fig. 1. The schematic diagram displayed in this figure is divided in three blocks delimited by dashes lines. The blocks are connected in a ring. The voltages v, v_a and v_b are the output and input signals for consecutive blocks. Let as describe how each block works. Let us describe the mode of operation of the circuit. In the block *B* the operational amplifier (op-amp in the follow) IC_3 works as a classical electronic integrator. The output of this type of integrators tends to wander off due to op-amp offsets and bias current because there is not feedback at direct current [40]. To solve this problems it is convenient to put a large resistor R_4 across the capacitor C_3 as it is shown in Fig. 1. In this case, by using the virtual ground approximation, the block *B* can be modeled by the follow equation

$$v_a = -R_3 C_3 \dot{v} - \frac{R_3}{R_4} v \tag{20}$$

where dot denote derivative with respect to the dimensional time. Note that in the limit $R_4 \to \infty$ the last term in Eq. (20) approaches to zero.

The block *A* can be describe by the follow second order differential equation [41]

$$v_b = b_2 \ddot{v}_a + b_1 \dot{v}_a + v_a \tag{21}$$

where the constants b_i $(i = 1, 2)$ depend on the circuit components according with

$$\begin{aligned} b_2 &= R_1 R_2 C_1 C_2 = (RC)^2 \\ b_1 &= (R_1 + R_2)C_2 + R_2 C_1 (1 - G) = (3 - G)RC \end{aligned} \tag{22}$$

where G is the gain for the circuit formed by IC_1 and P_1, which under virtual ground approximation is given by $G = P_1/P_g$ where P_g refers to the ohmic value of P_1 in between of the cursor of the potentiometer P_1 and ground. It is clear that the Eq. (21) can be modeled by using two integrators, however, the circuit represented in the block *A* provides a higher signal-to-noise ratio and better response in frequency domain than the corresponding circuit made with integrators. A more complete description of this circuit and a comparison with a circuit using two integrators can be found in Ref. [41]. The circuit shown in the block *A* has been used in researches in nonlinear dynamical system where the noise plays an important role (see for instance [42,43]).

For the nonlinear circuit (block C) we use the same one that in [39]. We included the adjustable resistor P_2 to play with the k parameter of Eq. (19), hence the relation between the voltages v' and v in block C of Fig. 1, under piecewise linear approximation of the current–voltage characteristic of the diodes, is given by

$$v' = D(v) = \begin{cases} -\frac{R_5}{P_2} v & if \quad v \le 0 \\ 0 & otherwise \end{cases} \tag{23}$$

and after the inverting amplifier IC_6, the block C can be described by

$$v_b = R_8 \left(\frac{v_0}{R_7} - \frac{D(v)}{R_6} \right) \tag{24}$$

where v_0 is an input constant voltage. Finally, take into account the previous equations describing each block we reach a three-order differential equation for the voltage v

$$(RC)^3 \dddot{v} + (RC)^2 (3 + \frac{R_3}{R_4} - G) \ddot{v} + (RC)[1 + \frac{R_3}{R_4}(3 - G)]\, \dot{v} + \frac{R_3}{R_4} v - \frac{R_8}{R_6} D(v) + \frac{R_8}{R_7} v_0 = 0. \tag{25}$$

With the follow definitions of the dimensionless variables

$$\tau = \frac{t}{RC}, \quad z = \frac{R_7}{R_8} \frac{v}{v_0}, \tag{26}$$

the identification of the parameters d_i in Eq. (18) given by

$$d_2 = 3 + d_0 - G,\ d_1 = 1 + d_0(3 - G),\ d_0 = \frac{R_3}{R_4}, \tag{27}$$

and defining the value of k in Eq. (19) by

$$k = \frac{R_8}{R_6} \frac{R_5}{P_2}, \tag{28}$$

the Eq. (25) transforms into the dimensionless Eq. (18). Note that as $d_0 = 10^{-2}$, it introduces a small correction to the coefficient values d_2 and d_1.

It is interesting to note that the scaled dimensionless variable z does not depend on the particular values of the parameters P_2 and G. Hence, different experimental realizations with different values of v_0 but with the same parameter values P_2 and G should be described by the same set of dimensionless parameters d_i of Eq. (27).

3.3. Technical details

The Eq. (26) defines a constant time $RC = 10^{-3}$ s^{-1} that determines the mean working frequency, $F \approx 140$ Hz. On the other hand, as $R_7 = R_8$, the scale factor given by Eq. (26) is just v_0. It is important to mention that the scale factor works under hypothesis of perfect piecewise linear function $D(x)$ having a not differentiable point at $x = 0$. As it was noted in [39], experimental realization of this function depends on the diode I–V curve, that shows a knee sharp rather than a not differentiable vertex-point. This fact will introduce some differences between scaled data of two *equivalent* experiments, as we will see in Section 6.

The data acquisition is take at 20 kilo samples per second with 16 bits precision and recording three channels, v, v_a and v_b. We used a NICOLET ODISSEY register to measure and to store data series in its hard discs. Later we transfer the data to a computer to be analyzed.

To reach the stationary behavior of the circuit and assure high precision, we switch on the circuit 40 min before to start the data series recording.

4. Experimental Poincaré map

The theory of intermittency presented in the Section 1 was developed for 1D maps, hence, to apply it to our continuous system we define a Poincaré map. Fig. 2(a) shows an experimental time series for the voltages v_a, v and v_d obtained from the points indicated in Fig. 1. Our experimental Poincaré map is determined by the intersection of the experimental trajectory of Fig. 2(a) with plane $v_a = 0$ passing from the subspace $v_a < 0$ to the subspace $v_a > 0$. This intersection take place in the rectangle shown in Fig. 2(a). It is also indicated the vertical line $v_a = 0$, $v = v_c$. The arrows going away from the line indicates the instability observed on the plane $v_a = 0$. The power spectra $S(f)$ is shown in Fig. 2(b) as a function of the frequency f. It was evaluated over a time series of 18×10^6 samples of $v(t)$. In Fig. 2(b) we can identified the main frequency $f_0 = 131$ Hz and the first sub-harmonic at $f_0/2$. This sub-harmonic is typical in type III intermittency and it is due to the alternating oscillation of the signal around the unstable point of the Poincaré map, that corresponds with the voltage v_c as the vertical line shows in Fig. 2(a). Figure Fig. 2(b) shows a continuous spectra corresponding with an irregular signal.

Fig. 3 shows experimental data for v_n, that is, the values of $v(t)$ intersecting the rectangle shown in Fig. 2. The obtained experimental Poincaré map given by v_n *vs* v_{n+1} is represented in Fig. 4.

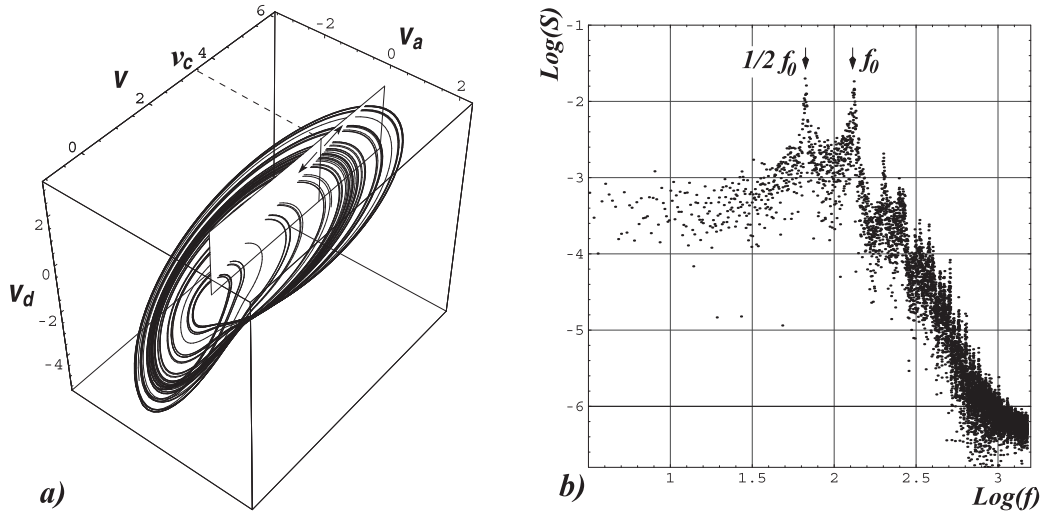

Fig. 2. (a) Experimental time series for $v_a(t)$, $v(t)$ and $v_d(t)$. The rectangle on the plane $v_a = 0$ used to define the Poincaré is also shown. On this rectangle it is displayed the vertical line $v_a = 0, v = v_c \approx 3.750$ V. For the arrows on the rectangle see main text. (b) Logarithmic plot of the Fourier power spectra. Arrows indicate the main frequency, $f_0 = 131$ Hz and the sub-harmonic at $f_0/2$. The circuit parameters are: $v_0 = 0.275$ V, $P_2 = 1.59$ kΩ and $G = 2.68$

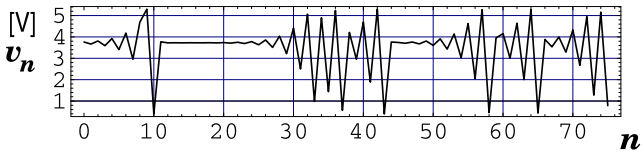

Fig. 3. Experimental values for v_n as a function of n showing laminar (around $v_c \approx 3.750$ V) and chaotic regions. It was represented only 75 points. The circuit parameters are the same that for Fig. 2.

Note that this figure is formed by a large density of data drawing a dark curve. The Poincaré map of Fig. 4 intersects with the bisector line at the fixed point v_c. A second map drawn by a low density data appears also in Fig. 4. It is formed by only a small number of data drawing the second return map, that is, x_{n+2} *vs* x_n. It due to some point which trajectories do not cross through the Poincaré plane during the precedent period. In other words, the Poincaré plane $v_a = 0$ is intersected by the trajectories in almost of the periods, but not for all of them, hence there are some lost experimental data. This is because in the data series x_n some points are not recorded. In such cases, it is represented x_{n+2} *vs* x_n instead x_{n+1} *vs* x_n.

The standard local map for this type of intermittency is given by Eq. (3) where $x = v - v_c$ and $p = 2$.

We estimate the local Poincaré map of Eq. (3) by fitting the points in a neighbor of the unstable fixed point by a second order polynomial $P(v)$ getting $P(v) = a_0 + a_1 v - a v^2 \approx 2.7V + 2.07v - 0.479V^{-1}v^2$. The local map is defined in a neighbor of the fixed point v_c given by the root of $P(v_c) = v_c$, hence by substituting $x = v - v_c$ into the original polynomial we get for the shifted voltage x the local Poincaré map of Eq. (3) with $p = 2$ as follow

$$x_{n+1} = P(x_n) = (a_1 - 2\,a\,v_c)x_n - a\,x_n^2 \tag{29}$$

where $a_2 = 0.48$ V^{-1}, $p = 2$ and $-(1+\varepsilon) = (a_1 - 2\,a\,v_c)$, providing the value $\varepsilon = 0.52$. We will need these experimental parameter values to estimate the probability density of the laminar length inside of the laminar region. Note that x_n in Eq. (29) has voltage dimension, but for sake of clarity, we retain the notation used in previous section for dimensionless variables.

As we mention before, Eqs. (18) and (25) describe a continuous system having more than one dimension but they can be described by the 1D map of Fig. 4. However, some comments are necessary at this point. Note that the map shown in Fig. 4 is a multivalued function and it can have a fractal structure. The first splitting of the Poincaé map associated with its fractal structure can be seen in the laminar region in Fig. 4. The upper branch correspond with the reinjection points whereas the lower one is the escape path for the reinjected points. Further fractal structure is difficult to identified due to the noise in the circuit. The parameter values of Eq. (29) are practically the same by considering the upper or the lower branch of the map, hence in the follow we consider that, in first approximation, the Poincaré map in as single-valued function.

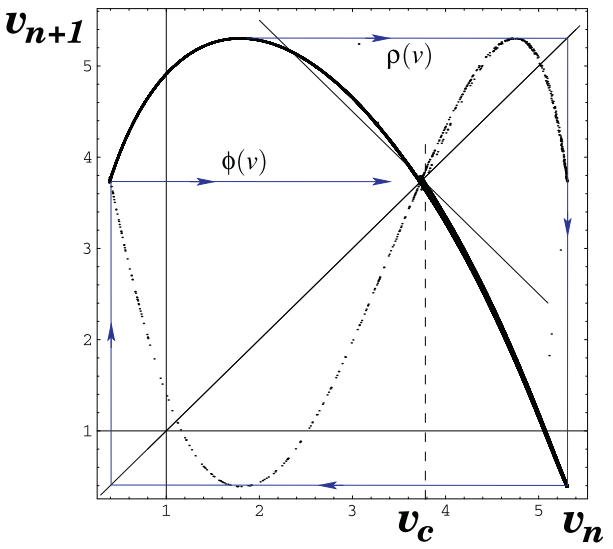

Fig. 4. Higher density of dots indicates the experimental Poincaré map. (For lower density see main text). Continuous black lines show the bisector one and the straight line with slope menus one passing thought the fixed point $v_c \approx 3.750$ V. Blue arrow shows a trajectory going from the maximum to the laminar region. The circuit parameters are: $v_0 = 0.275$ V, $P_2 = 1.59$ kΩ and $G = 2.68$. The number of plotted points is approximately 120,000. (For interpretation of the references to color in this figure legend, the reader is referred to the web version of this article.)

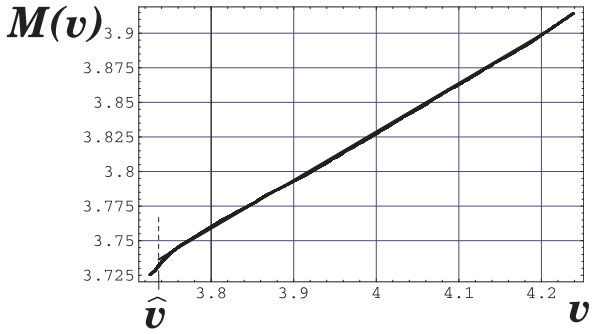

Fig. 5. Experimental function $M(v)$ for the map of Fig. 4 obtained by using the approximation (7). Dots correspond to experimental data and solid line show the corresponding least mean square fit given by $M(v) = 0.334v + 2.49V$. Dashed line indicates the value $\hat{v} = 3.739$ V, solution of $M(\hat{v}) = \hat{v}$.

5. Experimental estimation of the RPD

In this section we estimate the RPD associate to the map of Fig. 4 by following the procedure explained in Section 1. First of all, let us note that the experimental Poincaré map present indirect reinjection form the maximum to the laminar zone. In Fig. 4 it is shown by blue arrow the trajectory follows by a point starting closed to the maximum v_m, and arriving into the laminar zone. It is interesting to note that if the probability density around the maximum is uniform, then, after the first mapping it will be transformed into $\rho(v) \propto \Delta v_m^{\alpha}$ where Δv_m is the displacement from the maximum. The follow two iterations needed to get the laminar zone will preserve the mathematical shape of $\rho(v)$, hence the RPD indicated by $\phi(v)$ in Fig. 4 can be described by the power law (9) [19,20]. It is interesting to note that even the noise theory can be applied to this indirect reinjection [28].

By using the simple approximation given by Eq. (7) we get an experimental estimation of the function $M(v)$ associated to the Poincaré map shown in Fig. 4. The result is displayed in Fig. 5 confirms that the linear approximation of Eq. (8) works also for our continuous experimental system. Hence, by least mean square analysis we can calculate the values of the free parameters of the linear function $M(v) = m(v - \hat{v}) + \hat{v}$, getting $m \approx 0.334$ and $\hat{v} \approx 3.739$ V, in good agreement with the experimental data (see Fig. 5).

At this point, by using Eq. (9), we determine the RPD given by Eq. (4). The result is shown in Fig. 6 for the same data series used in Fig. 5, in good agreement with analytical prediction. Note that we does not fit the experimental data of Fig. 6, we just superimpose the power law given by Eq. (4) to the experimental data.

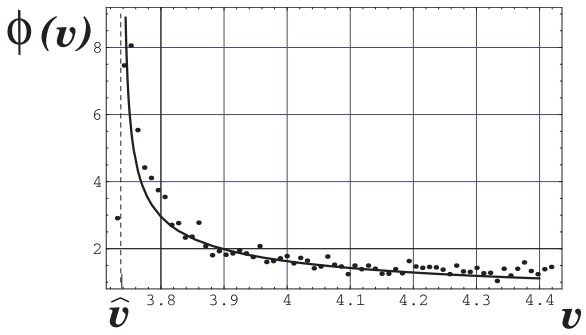

Fig. 6. RPD for the map of Fig. 4. Dots correspond to experimental data. Solid line correspond to Eq. (9) evaluated using the values of m and $\hat{v}$ of Fig. 5. Dashed line indicates the value $\hat{v} = 3.739$ V.

Note that $\hat{v}$ is the LBR, hence should not be reinjected point on the left of $\hat{v}$, indicated by the dashed line in Figs. 5 and 6. In fact, as we have $\alpha < 0$ the straight line $v = \hat{v}$ is a vertical asymptote for $\phi(v)$ and its graph does intersect the vertical line $v = \hat{v}$.

In this section we are focused on a low noise case, however the noise is always present in experiments, consequently, there are reinjected points failing in a small region on the left of $\hat{v}$, at it is shown in Fig. 6. In the Section 6 we study the noise effect on the RPD for a lower signal-to-noise ratio than in the actual case.

Regarding with the probability density of the laminar length ψ, Eq. (16) provides an analytical result depending on the RPD and the function $X(l, c)$. The free parameters ε and a determining $X(l, c)$ in Eq. (15) was found in Section 4 by fitting points of the Poincaré map near v_c, (see Eq. (29)). In this way we have determined the function $\psi(l)$ of Eq. (16) that represents the numerical data. The analytical plot is represented by a dashed line in Fig. 7, where we observe a deviation from the experimental data represented by dots. There are several effect contributing to this deviation. The more important one is that we have a relatively large value of ε, consequently, the classical approximation from the discrete map (3) to continuous one given by Eq. (12) is not so good. To increase the precision it is necessary to get a function $l(x, c)$ fitting the laminar duration l depending on the reinjected points x better than expression (13). To do this in a simple way, we can introduce a seed point x_s close to the fixed point x_c in the experimental map (29), then the iterated points $\{x_n\}$ of the starting x_s increase in a process driven by the experimental local map (29) until the trajectory goes out of the laminar region. The next step in to construct an interpolating function, let say $X(l, c)_{int}$, to approximate the data set $\{x_n, l_n\}$ where the l_n indicates the number of iterations needed for x_n to go out of the laminar region. Finally we can use in Eq. (16) the function $X(l, c)_{int}$ instead of $X(l, c)$. The result is shown by a solid line in Fig. 7 displaying better agreement with the experimental data that in the previous case.

6. Noise effect

The experimental data are affected by a noise produced by the measure procedure. Since $M(x)$ is defined by means of integrals, its numerical estimation is more robust reducing statistical fluctuations for noisy data. A different phenomenon studied here is that the behavior of the system changes due to the internal noise in the circuit as we indicate in Section 1. In this section we studies the noise effect on the RPD and $\psi(l)$, which is a novel topic in the intermittency theory because now the RPD is not a constant function.

For 1D maps have been reported the noise effect on the RPD function. An useful result is that, for region far from the fixed point, the slope of $M(v)$ is robust against the noise. This fact help us to find the RPD and the density $\psi(l)$ corresponding to the noiseless case, even from the noisy data. This is the key point to use Eq. (17) to estimate the NRPD.

Firstly, let us describe the procedure used to increase the noise in our dynamical system. In a first approximation, the internal noise strength in the circuit does not depend on the level of the signal. However, according with Eq. (26), the signal level is proportional to v_0. Consequently, to decrease the signal-to-noise ratio, we reduce the previous value from $v_0 = 0.275$ V to a new one $v_0 = 0.05$ V, whereas the rest of the parameters remain without change. With this procedure we have used the natural noise in the system without an additional noise generator. Fig. 8 shows two superimposed dimensionless data from experimental Poincarè maps corresponding to $v_0 = 0.275$ V and $v_0 = 0.05$ V. As we mention before, in the case of low signal, the diodes behavior differ slightly from large signal, hence the scaled functions $D(v)$ are not exactly the same in both cases. This is because that the corresponding scaled Poincaré maps differ approximately in a 10% and it is difficult to compare the laminar regions. To avoid this inconvenient and to compare much more clearly the laminar region between both experiments, instead v_0, we have used the value of the fixed point v_c as the normalizing factor (see Fig. 4). In this way, we use in Fig. 8 the dimensionless variable defined as

$$x = \frac{v}{v_c} - 1 \tag{30}$$

where we include -1 to shift the fix unstable point at $x = 0$. With this method, the largest deviations between both experiments appear at the top and at the bottom on of the maps. Following the procedure of the Section 5 we evaluate the function $M(x)$ for the experimental data corresponding to $v_0 = 0.05$ V. The experimental data are normalized by using Eq. (30) before they are represented in Fig. 9 together with the normalized data of Fig. 5. The vertical dashed lines in Figs. 9 and 10 indicate the corresponding values $\hat{x}$ obtained by fitting the subset of experimental data with $(x > 0)$. This values are also indicated in Fig. 9 by vertical dashes lines. In view of Fig. 9, some experimental results can be comment. Firstly we observe that for $x > 0$, that is for point far from $\hat{x}$, $M(x)$ is linear even in the case of large signal-to-noise relation (blue points in Fig. 9). Moreover according with analytical predictions, the found values of m are similar in both cases. More specific, in the case of $v_0 = 0.05$ V the least mean square analysis gives the follows values: $m_{0.05} = 0.374$ and $\hat{x}_{0.05} = -0.0324$, hence $m_{0.05}$ differs in 6% form the previous one $m = 0.350$, that is compatible with our not perfect piecewise function $D(x)$. Secondly, in the scaled plot of Fig. 9, the knee sharp region around the corresponding values of $\hat{x}$ increases as the signal-to-noise ratio decreases, hence for the $v_0 = 0.05$ V (blue points in Fig. 9) we observe a largest number of reinjected points on the left of $\hat{x}$ than for $v_0 = 0.275$ V case. This phenomenon produce the blue tail observed in Fig. 10 on the left of $\hat{x}$. Both phenomena are in agreement with the recently reported effect of the noise on the RPD in 1D maps. Concerning with the large signal-to-noise ratio case ($v_0 = 0.05$ V), the NRPD is given by Eq. (17) explained in Section 2.1, where $G(x - y, \sigma)$ is the probability density of the internal noise perturbing the experimental Poincaré map. This function is in general unknown, however, we can approach it as an uniform distributed noise as follows

$$G(x, \sigma) = \frac{\Theta(x + \sigma) - \Theta(x - \sigma)}{2\sigma}, \tag{31}$$

where $\Theta(x)$ is the Heaviside step function which is zero for negative argument and one for positive argument. Now, after evaluate the integral (17), the NRPD reaches

$$\Phi(x) = \begin{cases} 0 & x < \hat{x} - \sigma \\ \frac{b}{2\sigma(\alpha+1)}(x - \hat{x} + \sigma)^{\alpha+1} & \hat{x} - \sigma \le x \le \hat{x} + \sigma \\ \frac{b\left[(x-\hat{x}+\sigma)^{\alpha+1} - (x-\hat{x}-\sigma)^{\alpha+1}\right]}{2\sigma(\alpha+1)} & \hat{x} + \sigma < x \end{cases} \tag{32}$$

Some comments concerning with Eq. (32) can be do. Whereas the expression (31) has been previously used to evaluate Eq. (17) in the context of 1D maps having type I, II and III intermittency (see [23,24,28]), the result obtained here, Eq. (32), is different from the previous ones. This is because our Poincarè map is not a symmetric map as it happens in [28] for type-III intermittency and, on the other hand, there are not applied the usual border conditions to keep data in the domain of definition of the map, as it happen in numerical investigations with 1D maps (see for instance [24]). In our experimental dynamical system, the domain of definition of the Poincaré map is not imposed and is determined by the system itself.

The Eq. (32) has three free parameters, α, $\hat{x}$ and α, that we must to estimate. It is important to emphasize that the parameters $\hat{x}$ and σ in Eq. (32) determined the noiseless RPD of Eq. (4) used in the Section 5. As we mention before, the slope of $M(x)$ is robust against the noise, hence we can still use Eq. (9) to obtain α. The case of $\hat{x}$ is different and there is not a general method to evaluate from the noisy $M(x)$. For instance, for a noisy symmetric reinjection there is not a simple way to estimate the noiseless $\hat{x}$ [28], whereas for the map without symmetry considered in [23], it is proposed an estimation for $\hat{x}$.

Concerning with our experiment, it is clear that $\hat{x}$ is located at the middle of the interval $[\hat{x} - \sigma, \hat{x} + \sigma]$, and according with Eq. (32) the NRPD takes particular values at the endpoints of the interval. That is, $\Phi(\hat{x} - \sigma) = 0$ and Φ presents a vertex point at $x = \hat{x} + \sigma$, hence, we can estimate the value of σ and $\hat{x}$ from the experimental NRPD of Fig. 11 (dots). In this experiment, a good choice is $\hat{x} = \hat{x}_{0.05}$ and $\sigma \approx 0.013$ as it is indicated by vertical lines in Fig. 11. Eq. (32) is represented for this set of parameter values in good agreement with its experimental estimation. It is interesting to note that in this experiment the whole function $M(x)$ is robust against the noise, not just its slope. To show clearly the noise effect on the RPD, in Fig. 11 is superimposed in dashes line the RPD of Eq. (4), in other word, the RPD that should be observed in an ideal noiseless experiment. In this case the straight line $x = \hat{x}$ should be a vertical asymptote for $\phi(x)$. Concerning with the noisy density of laminar length we can still use Eq. (16). It is only necessary substitute $\phi(X(l, c))$ by $\Phi(X(l, c))$ gives by Eq. (32). A comparison with experimental data is shown in Fig. 12. As in the noiseless case of Fig. 7 we present two analytical plots using the functions $X(l, c)_{int}$ and $X(l, c)$. As in the noiseless case, we obtain better agreement by using $X(l, c)_{int}$.

7. Conclusions

In this work we have shown that the generalized of reinjection probability density (RPD) used for 1D-maps provides faithful description of intermittencies in continuous experimental systems. Such RPD, taken in the form of a power-law function.

First of all, to apply the theory we defined a Poincaré section in the phase space on the continuous experimental system.

Calculation of the RPD in 1D map having chaotic intermittency is based on the earlier introduced integral characteristic $M(x)$. We have shown that, even in our continuous experimental system, $M(x)$ is a linear function: $M(x) = m(x - \hat{x}) + \hat{x}$ where the free parameters $\hat{x}$, that is the LBR, and $m \in (0, 1)$ determine the type of RPD. We found a good agreement with the experimental data. This means that generalized RPD also driven the reinjection process in our analog circuit experiment.

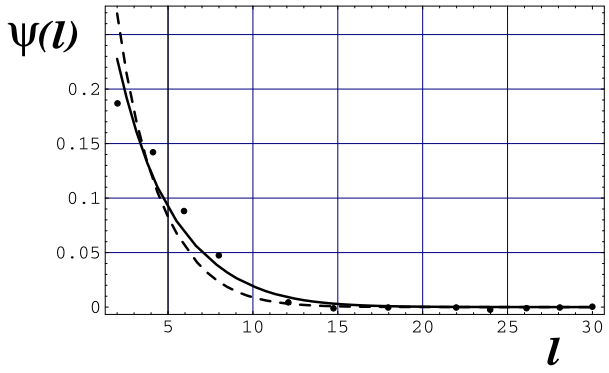

Fig. 7. Dots indicate the experimental probability density of laminar length. Lines represents $\psi(l)$ given by Eq. (16), where in solid lines is used the function $X(l, c)$ given by Eq. (16), whereas for dashes line we have used $X(l, c)_{int}$ as it is described in the main text.

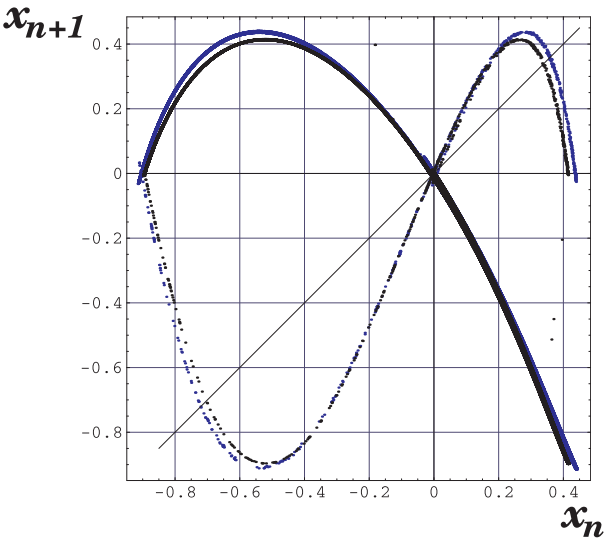

Fig. 8. Dimensionless data by using Eq. (30) that correspond to two experimental Poincaré maps with different signal-to-noise ratio. Black dots correspond with data of Fig. 4. Blue dots are the same but for $v_0 = 0.05$ V. Continuous line show the bisector one. (For interpretation of the references to color in this figure legend, the reader is referred to the web version of this article.)

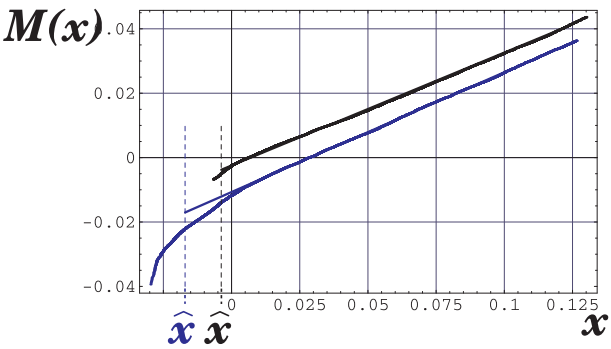

Fig. 9. Experimental functions $M(x)$ for the maps represented in Fig. 8. Black color indicates the case $v_0 = 0.275$ V whereas blue color refers to $v_0 = 0.05$ V. Dots correspond to experimental data and solid lines show the corresponding least mean square fit. Vertical dashed line indicate the corresponding values for the LBRs. (For interpretation of the references to color in this figure legend, the reader is referred to the web version of this article.)

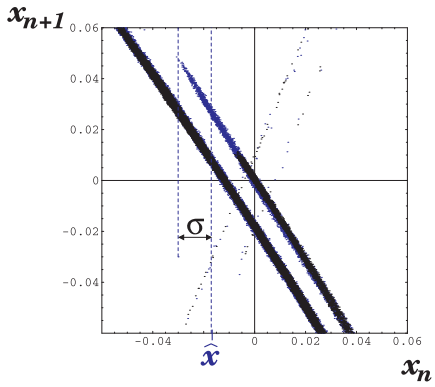

Fig. 10. A magnification of the laminar region of Fig. 8. For vertical dashed lines, see main text. Black color indicates the case $v_0 = 0.275$ V whereas blue color refers to $v_0 = 0.05$ V. (For interpretation of the references to color in this figure legend, the reader is referred to the web version of this article.)

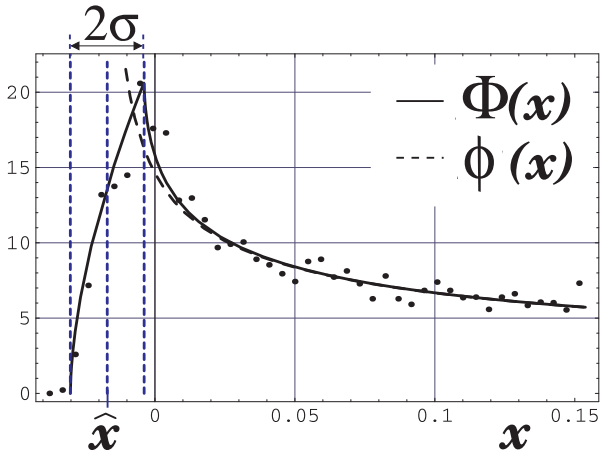

Fig. 11. NRPD for the map of Fig. 8. Dots correspond to experimental data. Solid line correspond to the analytical expression Eq. (32) evaluated using the values of m and $\hat{x}$ of Fig. 9. Dashes curve indicates the ideal noiseless RPD.

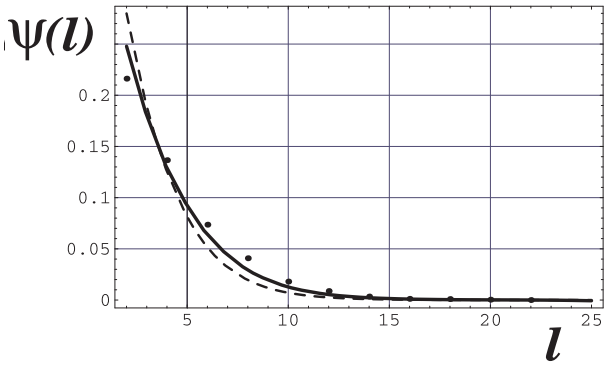

Fig. 12. Dots indicate the experimental probability density of laminar length for $v_0 = 0.05$ V. Dashes line represents $\psi(l)$ given by Eq. (16), where ϕ was substituted by Φ. As in Fig. 7, for solid line we have used $X(l, c)_{int}$ instead $X(l, c)$.

The function $M(x)$ determines the power-law RPD, $\phi(x) = (x - \hat{x})^{\alpha}$. In this case we also found a good agreement with the experimental reinjection probability density.

Furthermore, from the generalized RPD we can derived an analytical expression for the probability density of the laminar length, $\psi(l)$, showing good agreement with the experimental data. The chosen experimental system was based on the proposed system in Ref. [39]. An important property of this system is that it is easy to scale by tuning the voltage v_0, hence we used this feature to decrease the signal-to-noise ratio. This fact have been used to study the effect of the natural noise in the circuit and to compare with the theoretical predictions. To study the effect of noise we have used the methodology

recently developed for the noisy 1D map having intermittency. That is, after making an experimental evaluation of the function $M(x)$ by fitting the noisy data set, we use this to obtain the noisy reinjection probability density (NRPD) corresponding to the higher signal-to-noise ratio experiment. We propose an analytical description of the NRPD in a good agreement with the experimental data. It is also important to note, that the function $M(x)$ obtained from noisy data provides a complete description of the RPD for an ideal noiseless system. In the noisy experiment we also have found a good agreement between the analytical probability density of the laminar length and the experimental data series.

Note that the power-law RPD is generated in the maximum of the experimental Poincaré map, and after two iterations, the points closed to the maximum are mapped into the laminar zone, so we have an indirect reinjection (see Fig. 4). In spite of this fact, we found good agreement with the experimental data in both cases, with and without noise.

Acknowledgments

This research is supported the Spanish Ministry of Science and Innovation (MICINN) under Project No. ESP2013-41078-R (EdR) and the CONICET under Project No. PIP 11220090100809, and by National University of Córdoba, Argentina (SE) and by Universidad Politécnica de Madrid.

References

[1] Manneville P, Pomeau Y. Phys Lett A 1979;75:1–2.
[2] Pomeau Y, Manneville P. Intermittent transition to turbulence in dissipative dynamical systems. Commun Math Phys 1980;74:189–97.
[3] Dubois M, Rubio M, Berge P. Experimental evidence of intermittencies associated with a subharmonic bifurcation. Phys Rev Lett 1983;51:1446–9.
[4] Stavrinides SG, Miliou AN, Laopoulos Th, Anagnostopoulos AN. The intermittercy route to chaos of an electronic digital oscillator. Int J Bifurcation Chaos 2008;18:1561–6.
[5] Zebrowski J, Baranowski R. Type i intermittency in nonstationary systems models and human heart rate variability. Physica A 2004;336:74–83.
[6] Chian A. Complex systems approach to economic dynamics. In: Lecture notes in economics and mathematical systems, 592. Berlin: Springer; 2007. p. 39–50.
[7] Schuste H, Just W. Deterministic chaos. An introduction. Weinheim, Germany: Wiley-Vch Verlag GmbH & Co. KGaA; 2005.
[8] Hirsch JE, Nauenberg M, Scalapino DJ. Intermittency in the presence of noise: a renormalization group formulation. Phys Lett A 1982;87:391–3.
[9] del Rio E, Elaskar S. New characteristic relations in type-II intermittency. Int J Bifurcation Chaos 2010;20:1185–91.
[10] del Rio E, Elaskar S, Donoso JM. Laminar length and characteristic relation in type-i intermittency. Commun Nonlinear Sci Numer Simulat 2014;19:967–76.
[11] Elaskar S, del Rio E. New advances on chaotic intermittency and its applications. Springer; 2017.
[12] Manneville P. Intermittency, self-similarity and 1/f spectrum in dissipative dynamical systems. Le J Phys 1980;41:1235–43.
[13] Pikovsky A, Osipov G, Rosenblum M, Zaks M, Kurths J. Attractor-repeller collision and eyelet intermittency at the transition to phase synchronization. Phys Rev Lett 1997;79:47–50.
[14] Kim CM, Kwon OJ, Lee E-K, Lee H. New characteristic relations in type-i intermittency. Phys Rev Lett 1994;73:525–8.
[15] Kim CM, Yim GS, Ryu JW, Park YJ. Characteristic relations of type-III intermittency in an electronic circuit. Phys Rev Lett 1998;80:5317–20.
[16] Cho JH, Ko MS, Park YJ, Kim CM. Experimental observation of the characteristic relations of type-i intermittency in the presence of noise. Phys Rev E 2002;65:036222.
[17] Kye WH, Rim S, Kim CM, Lee JH, Ryu JW, Yeom BS, Park YJ. Phys Rev E 2003;68:036203.
[18] Koronovskii AA, Hramov AE. Type-II intermittency characteristics in the presence of noise. Eur Phys J B 2008;62:447–52.
[19] Elaskar S, del Rio E, Donoso JM. Reinjection probability density in type-III intermittency. Physica A 2011;390:2759–68.
[20] del Rio E, Elaskar S. On the theory of intermittency in 1d map. Int J Bifurcation Chaos 2016;26:1650228.
[21] Kim CM, Yim GS, Kim YS, Kim JM, Lee HW. Experimental evidence of characteristic relations of type-i intermittency in an electronic circuit. Phys Rev E 1997;56:2573–7.
[22] del Rio E, Elaskar S, Makarov A. Theory of intermittency applied to classical pathological cases. Chaos 2013;23:033112.
[23] Krause G, Elaskar S, del Rio E. Noise effect on statistical properties of type-i intermittency. Physica A 2013;402:318.
[24] Elaskar S, del Rio E, Krause G, Costa A. Effect of the lower boundary of reinjection and noise in type-II intermittency. Nonlinear Dyn 2015;79:1411–24.
[25] Elaskar S, del Rio E, Costa A. Reinjection probability density for type-III intermittency with noise and lower boundary of reinjection. J Comput Nonlinear Dyn 2017;12. 031020–031020
[26] Hirsch JE, Huberman BA, Scalapino DJ. Theory of intermittency. Phys Rev A 1982;25:519–32.
[27] Pikovsky AS. J Phys A 1983;16:L109.
[28] del Rio E, Sanjuán MAF, Elaskar S. Effect of noise on the reinjection probability density in intermittency. Commun Nonlinear Sci Numer Simulat 2012;17:3587–96.
[29] Ott E. Caos in dynamical systems. Cambridge: Cambridge University Press; 2008.
[30] Franck C, Klinger T, Piel A. Intermittency or noise - an experimental study on the ion-beam driven ion-acoustic instability. Phys Lett A 1999;259:152–7.
[31] Hugo LDdeS, Cavalcante S, Leite JRR. Averages and critical exponents in type-III intermittent chaos. Phys Rev E 2002;66:026210.
[32] Stemler T, Werner JP, Benner H, Just W. Stochastic modelling of intermittency. Phil Trans R Soc A 2010;368:273–84.
[33] Stan C, Cristescu CP, Dimitriu DG. Analysis of the intermittent behavior in a low-temperature discharge plasma by recurrence plot quantification. Phys Plasmas 2010;17:042115.
[34] Ono Y, Fukushima K, Yazaki T. Critical behavior for the onset of type-III intermittency observed in an electronic circuit. Phys Rev E 1995;52:4520–3.
[35] Chua L, Lin G. Intermittency in a piecewise-linear circuit. IEEE Trans Circuit Syst 1991;38:510–20.
[36] Kye W, Rim S, Kim Ch. Experimental observation of characteristic relations of type-III intermittency in the presence of noise in a simple electronic circuit. Phys Rev E 2003;68:036203.
[37] Hramov AE, Makarov VV, Maximenko VA, Koronovskii AA, Balanov AG. Intermittency route to chaos and broadband high-frequency generation in semiconductor superlattice coupled to external resonator. Phys Rev E 2015;92:022911.
[38] Manffra EF, Caldas IL, Viana RL, Kalinowski HJ. Type-i intermittency and crisis-induced intermittency in a semiconductor laser under injection current modulation. Nonlinear Dyn 2002;27:185–95.
[39] Kiersa K, Schmidtb D. Precision measurements of a simple chaotic circuit. Am J Phys 2004;72:503–9.
[40] Horowitz P, Hill W. The art of electronics. Second edition. New York: Cambridge University Press; 1989.
[41] del Rio E, Rodriguez-Lozano A, Velarde MG. A prototype helmholtz-thompson nonlinear oscillator. Rev Sci Instrum 1992;63:4208–12.
[42] del Rio E, Rodriguez-Lozano A, Velarde MG. Melnikov criterion and its experimental test using a nonlinear oscillator. Chaos Solitons Fractals 1994;4:255–62.
[43] del Rio E, Sanmartin JR, Lopez-Rebollal O. Experimental evidence of a hard transition to chaos. Int J Bifurcation Chaos 1998;18:2225–62.